GEOPHYSICS, VOL. 52, NO. 8 (AUGUST 1987); P. 1065-1073, 8 FIGS., 1 TABLE.

Seismic wave synthesis by Gaussian beam summation: A comparison with finite differences

Th. George*, J. Virieux*, and R. Madariaga*

ABSTRACT

We apply Gaussian beam summation to the calculation of seismic reflections from complex interfaces, introducing several modifications of the original method. First, we use local geographical coordinates for the representation of paraxial rays in the vicinity of the recording surface. In this way we avoid the time-consuming evaluation of the ray-centered coordinates of the observation points. Second, we propose a method for selecting the beams that ensures numerical stability of the synthetic seismograms. Third, we introduce a simple source wave packet that simplifies and stabilizes the calculations of inverse Fourier transforms.

We compare reflection seismograms computed using the Gaussian beam-summation method with those calculated by finite differences. Two simple models are used. The first is a continuous curved interface separating an elastic layer from a free half-space. A double caustic, or degenerate focal point, appears due to the crossing of reflected rays. In this instance the finite-difference simulation and the Gaussian beam summation are in excellent agreement. Both phase and amplitude are modeled correctly for both the direct and reverse branches. When compared to geometrical ray theory, Gaussian beam summation provides a good approximation of the field near the caustics while geometrical ray theory does not. The second, more complex, model we consider is a trapezoidal dome with sharp corners in the interface. The corners of the dome in this model produce rather strong diffractions. Also, creeping head waves propagate along the interface. The results compare well with the finite-difference simulation except for the diffracted branches, where the traveltime of diffracted waves is poorly approximated by the Gaussian beam-summation method.

INTRODUCTION

Katchalov and Popov (1981) and Červený et al. (1982) recently proposed the use of a sum of Gaussian beams as a method for the numerical synthesis of seismograms in complex heterogeneous media. Although the theoretical foundation for the method is incomplete, several authors have shown that Gaussian beam summation works for simple geometrical models and that it yields results that compare favorably with exact solutions when they are available, or with numerical computations obtained by other techniques. See, for instance, Červený and Klimes (1984), Nowack and Aki (1984), Madariaga and Papadimitriou (1985), and Beydoun and Ben-Menahem (1985). As shown by Madariaga (1984), Gaussian beams are an analytical continuation of the Maslov, or WKB, techniques to complex values of the apparent slowness. The field at the source is decomposed into a series of beams and then each beam is propagated independently using the paraxial ray approximation (see, e.g., Červený and Pšenčik, 1984).

In order to use Gaussian beams, two problems have to be solved. First, the source has to be decomposed into a sum of Gaussian beams. This problem has been discussed by Červený et al. (1982), Madariaga (1984), and Madariaga and Papadimitriou (1985) who obtained the decomposition of general moment tensor sources. The problems of propagation, reflection, and refraction of Gaussian beams were discussed by Červený et al. (1982), Cisternas et al. (1984), and Babich et al. (1984). The latter authors give a new approach to Gaussian beam theory that is much simpler than the parabolic equation method originally introduced by Babich and Pankratova (1973).

METHOD

We very closely follow the development of the Gaussian beam technique as presented by Červený et al. (1982). The

Manuscript received by the Editor January 27, 1986; revised manuscript received January 16, 1987.
*Laboratoire de Sismologie, Institut de Physique du Globe de Paris, 4 Place Jussieu, F 75230, Paris 05, France.

notation is the same. A synthetic acoustic seismogram is given by the sum

$$u(M, \omega) = \int_{\phi_2}^{\phi_1} \Phi(\phi)\, \Pi(\phi)\, A(\phi)\, e^{-i\omega\theta(\phi)}\, d\phi, \qquad (1)$$

where ω is the frequency, M is the observation point, ϕ is the takeoff angle of the central ray (see Figure 1), ϕ_1 and ϕ_2 are the limits of the sum of Gaussian beams, and $\Phi(\phi)$ is the excitation factor of the source. Complete expressions of Φ for moment tensor sources may be found in Madariaga and Papadimitriou (1985). $\Pi(\phi)$ contains the product of all the reflection and transmission coefficients at the interfaces encountered by the beam along its trajectory.

The complex beam amplitude and phase are given by

$$A = \left(\frac{i\varepsilon\rho_0 v_0}{2\rho v q}\right)^{1/2}$$

and

$$\theta = \tau + \frac{p}{q}\frac{n^2}{2}, \qquad (2)$$

where ρ and v are density and velocity of the medium at the observation point, ρ_0 is the corresponding value at the source, and ε is explained below. The normal distance from the point M to the central ray n is defined in Figure 1.

The conjugate canonical functions q and p are

$$\begin{pmatrix} q \\ p \end{pmatrix} = \varepsilon \begin{pmatrix} q_1 \\ p_1 \end{pmatrix} + \begin{pmatrix} q_2 \\ p_2 \end{pmatrix}, \qquad (3)$$

where (q_1, p_1) and (q_2, p_2) are two fundamental solutions of the paraxial ray approximation equations (also called dynamic ray tracing by Červený and Hron, 1980) computed along the ray ϕ. The first solution corresponds to the "plane" wave initial condition, and the second solution corresponds to a point source. The latter provides the usual geometrical spreading for point sources. The complex parameter ε defines the spread of Gaussian beams in the direction perpendicular to the central ray. In homogeneous media, Červený et al. (1982) showed that Im (ε) was a measure of the beam width at the waist located a distance Re (ε) from the origin of the coordinate. For general heterogeneous media, ε has no clear meaning.

At interfaces, p and q are connected by the formulas developed by Červený (1983), and the transmission and reflection coefficients are calculated at the point where the central ray impinges on the interface.

The time-domain equivalent of equation (1) is

$$u(M, t) = \frac{1}{\pi}\int_{\phi_2}^{\phi_1} \mathrm{Re}\left[\Phi(\phi)\, \Pi(\phi)\, A(\phi)\, \frac{1}{t - \theta'}\right] d\phi, \qquad (4)$$

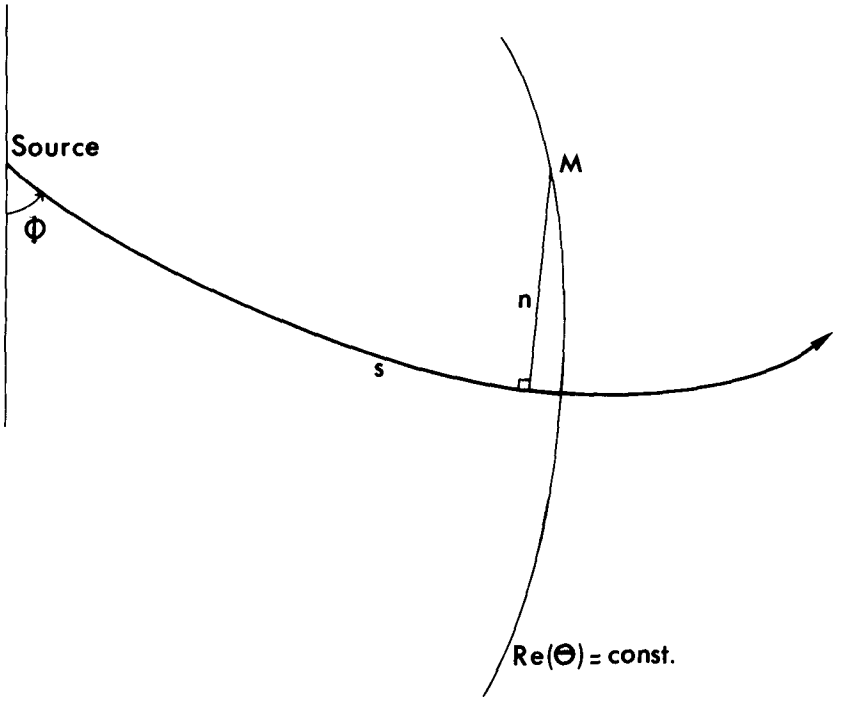

FIG. 1. Definition of the ray-centered coordinate (s, n): s measures the arc length along the ray from the source to the projection of the ray at the observation point M. n is the distance from the point M to the ray. Re (θ) = constant is the wavefront of the beam.

where $\theta' = \theta + ia$, and a is a finite smoothing time. This is necessary to eliminate the singularity in equation (4) when $t \to \theta'$, which occurs when the central ray passes close to the receiver at M. As shown by Madariaga and Papadimitriou (1985), use of this imaginary perturbation to the phase θ is equivalent to using an elementary source function of the type

$$f(t) = \frac{1}{\pi} \frac{a}{t^2 + a^2}. \tag{5}$$

Equation (4) is the basic expression used here to evaluate synthetic seismograms. Each term under the integral is the contribution of an individual Gaussian beam to the synthetic seismogram at M. Each one of these Gaussian beams is denoted by the takeoff angle ϕ of the central ray of the beam.

Designate ϕ_0 as the central ray which passes through the receiver at M. This is the classical ray joining the source to M. For this ray, the complex phase defined in equation (2) is $\theta(\phi_0) = \tau(\phi_0) = \tau_0$, since $n = 0$. For any other central ray in its vicinity, the phase of the beam is

$$\theta_\phi = \tau_\phi + \frac{1}{2}\left(\frac{p}{q}\right) n_\phi^2, \tag{6}$$

where the index ϕ indicates that τ, p, q, and n depend on the central ray under consideration. From paraxial ray theory (Červený and Hron, 1980; Červený and Klimes, 1984),

$$\frac{dn_\phi}{d\phi} = q_2(\phi_0),$$

so that

$$n_\phi \simeq q_2(\phi - \phi_0) \tag{7}$$

in the vicinity of the geometrical ray ϕ_0. Also, at $n_\phi = 0$,

$$\frac{d\tau}{dn} = 0,$$

$$\frac{d^2\tau}{dn^2} = -\frac{p_2}{q_2}, \tag{8}$$

and

$$\frac{d\theta}{dn} = 0.$$

Then, taking the second derivative of equation (6) and using the above results, we find that

$$\frac{d^2\theta}{dn^2} = \frac{p}{q} - \frac{p_2}{q_2} = \theta''.$$

Expanding θ_ϕ in a Taylor series about ϕ_0, we get

$$\Delta\theta_\phi = \theta_\phi - \theta_{\phi_0} = \theta'' \frac{n^2}{2},$$

so that finally, using equation (7), we obtain

$$\theta_\phi = \tau(\phi_0) + \tfrac{1}{2}\theta'' q_2^2 (\phi - \phi_0)^2. \tag{9}$$

Equation (9) relates the complex phase $\theta(\phi)$ to the takeoff angle ϕ at the source for the beams in the vicinity of the geometrical ray ϕ_0. It may be used to prove that the saddle-point approximation to equation (1) yields the ray-theoretical approximation

$$u(M, \omega) = \Phi(\phi_0)\, \Pi(\phi_0) \left[\frac{\rho_0 v_0}{\rho v q_2(\phi_0)}\right]^{1/2} e^{i\omega\tau_0} \frac{\sqrt{\pi}}{\sqrt{\omega}} e^{i\pi/4}, \tag{10}$$

where ϕ_0 defines the geometrical ray passing through the observation point M.

Numerical evaluation of equation (4) consists in discretizing it choosing a set of central rays ϕ_i so that equation (1) is replaced by

$$u(M, t) = \frac{1}{\pi} \sum_i \mathrm{Re}\left\{\Phi(\phi_i)\, \Pi(\phi_i)\, A(\phi_i) \frac{1}{t - \theta_i'}\right\} \Delta\phi_i. \tag{11}$$

If we choose steps $\Delta\phi_i$ of constant takeoff angle for the central rays, they appear at the surface with variable spacing. As a result, the numerical results will be good where the ray density is high and poor elsewhere. In order to improve the numerical stability of the sum (11), we choose the central rays so that they intercept the surface at relatively regular intervals. For this purpose we use equation (7) which relates $\Delta\phi$ to Δn. If the ray impinges on the recording surface with an incidence angle ψ, then $\Delta x = \Delta n \cos(\psi)$ and, from equation (7),

$$\Delta\phi = \frac{\Delta x \cos(\psi)}{q_2}. \tag{12}$$

In practice we choose Δx by trial and error, but a good rule of thumb is that Δx should be less than one-half the dominant wavelength of the source wave packet.

Equation (2) includes the distance n from *every* observation point to the central ray of *every* Gaussian beam. This is a difficult mathematical problem that has to be solved by numerical methods. As shown by Madariaga (1984), it is much more economical to use local geographical coordinates in the vicinity of the observation point. For that purpose, we introduce a local contact transformation from (q, p) in ray-centered coordinates to the corresponding set of canonical variables (ξ, η) in geographical coordinates. θ may also be easily expressed in the new variables. Červený (1984) found similar results using coordinate transformations and phase matching at the interface.

Ray tracing and the computation of the fundamental solutions (q_1, p_1) and (q_2, p_2) of the paraxial ray equations were obtained using the program RAY81 written by Červený and Pšenčík (1984). In order to save computer time, synthetics are calculated only in a time window for which there is a significant contribution of the beams to the sum (4). The smoothing parameter a in equation (5) was chosen equal to the step Δt. Finally, the beam "width" parameter ε was chosen as suggested by Červený et al. (1982) as

$$\varepsilon = i\,|q_2/q_1|,$$

but it was averaged over a number of central rays passing in the vicinity of the observer.

In the case of the corner model, we calculated synthetics using the Maslov approximation by making ε very large. As shown by Madariaga (1984), when the proper initial conditions are used for the fundamental solution (q_1, p_1), the Gaussian beam method reduces to Maslov's method at the source (see Chapman and Drummond, 1982).

GEOMETRY OF THE MODELS

We consider two models consisting of a single homogeneous layer overlying a homogeneous half-space. A complex interface separates the two media. Although more complex models incorporating both *P*- and *SV*-waves may be studied, we have deliberately kept complexity at a minimum in order to isolate the main features of reflection seismograms. A point source is located on the free surface. The vertical axis points downward into the medium, and the offset distance is measured along the free surface from the source. We consider seismograms recorded at geophones located only on the free surface.

The reflector shape is chosen to be complex enough to produce several different types of wave phenomena of interest in seismic modeling, namely, reflections, caustics, diffractions, and creeping head waves. Two basic interfaces are considered, the first being a smooth curved interface which produces a double caustic at the free surface, and the second, an interface with sharp corners which produces strong multiply diffracted waves. These two models are shown in Figure 2. The first model is referred to as the "cusp" model, while the second one is called the "corner" model. The velocity and density of the media are presented in Table 1.

Table 1. Physical properties of the models.

		Cusp	Corner
Velocity	Layer	3.46 km/s	2.5 km/s
	Half-space	—	4 km/s
Density	Layer	2.5 kg/dm^3	2.6 kg/dm^3
	Half-space	—	3.1 kg/dm^3
Source characteristics	α	4 S^{-2}	1000 S^{-2}
	t_0	1.35 S	.2 S
	Peak frequency	.8 Hz	13 Hz
	Upper half-power frequency	1.5 Hz	16.5 Hz

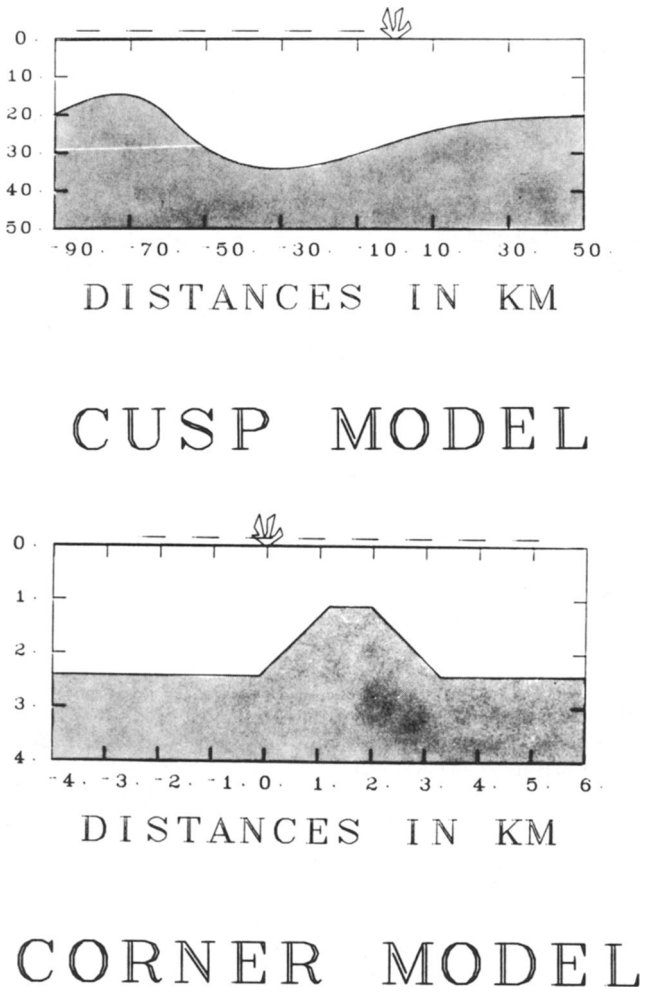

FIG. 2. Geometry of the models. The half-space is grey. The source is located at the origin of coordinates, and the receivers are indicated by the dotted line along the free surface.

Waves are emitted from a source at the free surface within a frequency window chosen so as to satisfy the requirements of the high-frequency ray approximation, and to allow computation with a low-frequency method such as finite differences (Virieux, 1984, 1986). The frequency content is controlled with the following source function:

$$s(t) = (t - t_0)e^{-\alpha(t-t_0)^2},$$

where t_0 is a time shift chosen to obtain a causal signal: $s(t) \simeq 0$ for $t < 0$, and α is related to peak frequency ($.39\sqrt{\alpha}$) and the upper half-power frequency ($.528\sqrt{\alpha}$) of the source spectrum (Alford et al., 1974). These quantities are given in Table 1.

Because we are only interested in waves reflected by the interface, the direct waves had to be eliminated from the finite-difference seismograms. They were eliminated by substracting from the seismogram for the complete medium the seismograms obtained for a finite-difference simulation of a homogeneous half-space with the same physical parameters as the upper medium. This subtraction also removes the spurious reflections produced by the two vertical sides of the finite-difference grid, but it does not eliminate the reflections of these spurious waves by the interface.

In the cusp model, our first example, we focus attention on the computation of the reflected waves near the bright spot produced by the intersection of the caustics with the free surface. To avoid problems with critically reflected waves, we consider that the interface is free, i.e., the lower medium does not exist. For the corner model, the sharp corners of the interface produce diffraction. The two media are considered to be elastic since this allows us to compare the amplitudes of diffracted waves with respect to creeping head waves. Using these two examples, and comparing their solutions by finite differences and Gaussian beam summation, we determine the validity of the latter method.

THE CUSP MODEL WITH A FREE INTERFACE

The comparison between Gaussian beam summation and finite differences starts with a simple model where the smooth curved interface is free. The free-boundary conditions were obtained by setting the shear modulus of the lower medium equal to zero for finite differences, and by choosing a reflection coefficient of -1 in Gaussian beam summation. The frequency range of synthetics (see Table 1) is low enough for finite-difference modeling to be valid, and high enough with respect to the wavelength of spatial variations of the interface so that Gaussian beam summation may be applied.

The curvature of the interface produces a double caustic (or "swallow tail") of reflected waves. These two caustics intersect at a focal point at a depth of 18 km, and they appear on the free surface at -47 km and -67 km, as shown in Figure 3. Ray theory breaks down in the vicinity of the two caustics where infinite amplitudes are obtained. Between these caustics there is a triplication of arrival times as shown in Figure 3. Branch 1 is the wave reflected beneath the source, while branch 3 is the wave reflected from the shallow part of the interface. Note the high density of rays leaving the source that is needed to ensure a correct density of exit points for the modeling of branch 3. Branch 2 is expected to have a strong amplitude because of its proximity to the focal point.

Three seismic profiles are presented for this geometry in Figure 4. The first profile (a) was obtained by finite differences. The second one (b) is the Gaussian beam-summation profile, while the third profile (c) was obtained from geometrical ray theory, avoiding the immediate vicinity of the caustics where this method breaks down. The low-frequency signal used to keep finite-difference costs at a reasonable level somewhat hides the separation of the three branches, but they are quite clear in the ray-theoretical seismograms.

The agreement between finite differences and Gaussian beam summation is quite good in this example. From Gaussian beam-summation modeling, we can see that the strong amplitude observed near the triplication comes from branch 2. The diffraction from the caustics, with its rapid decrease of amplitude, is correctly modeled by Gaussian beam summation. This means that the parabolic wavefront of individual Gaussian beams in Gaussian beam summation is a good approximation for this type of diffraction. The approximation for the case of diffraction by a reflector with discontinuities is not as good, as will be discussed in the next section. The asymmetry between the diffraction from either of the caustics may be explained by variations of the angle of reflection at the interface. As seen in Figure 3, this angle is nearly normal for the caustic at -47 km, producing a strong amplitude in a narrow range of offsets; however, the angle is close to 45 degrees for the caustic at -67 km, spreading the diffraction on a wider range.

The ray-theoretical seismograms, shown in Figure 3c, quite clearly show that the reverse branch (number 2) is Hilbert transformed (90 degrees out of phase) with respect to the direct phases of branches 1 and 3. The agreement between the three figures inside the domain of applicability of ray theory is excellent and demonstrates the validity of finite-difference and Gaussian beam summation in these "classical" areas. If we take the finite-difference simulation as exact within the frequency range under consideration, then Gaussian beam sum-

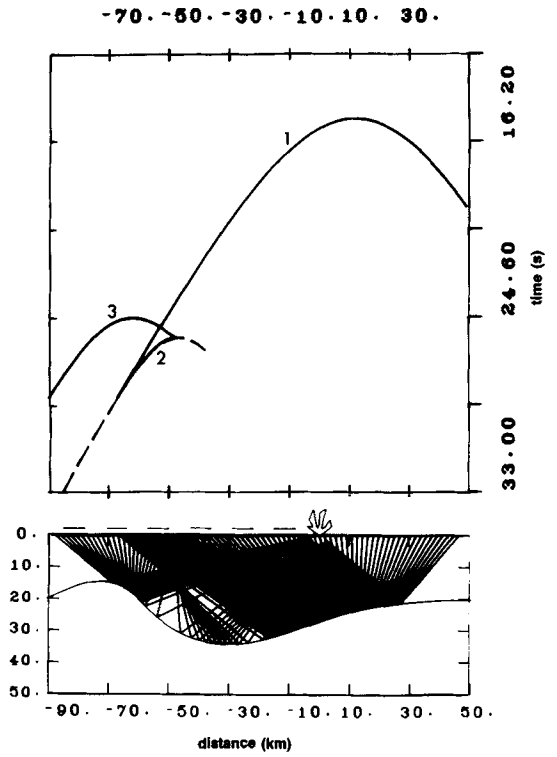

FIG. 3. Cusp model: ray diagrams and traveltime curves recorded at the free surface.

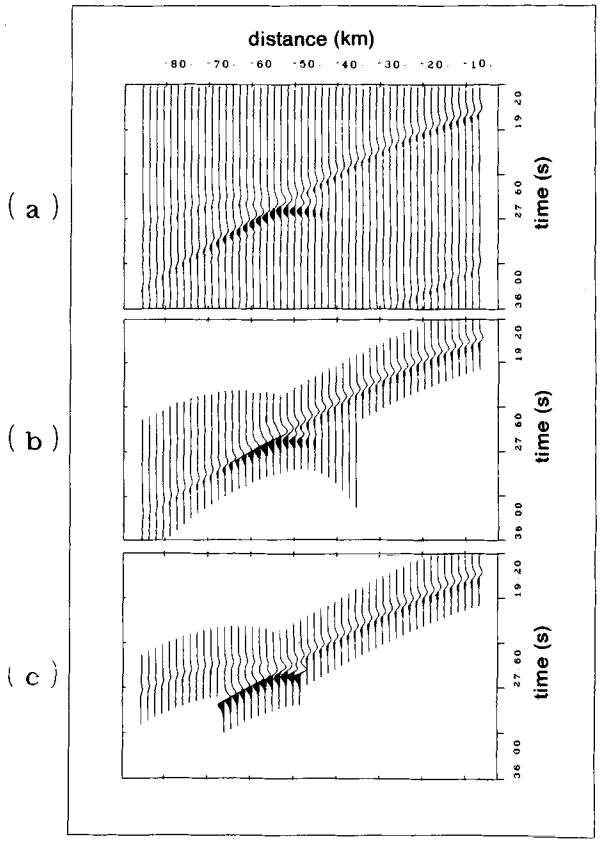

FIG. 4. Results for the cusp model: Seismic profiles are calculated (a) by finite differences, (b) by Gaussian beam summation, and (c) by geometrical ray theory.

mation also gives good results even beyond the caustics, in the Fresnel zones of caustic diffraction. This extends and confirms the results of Červený et al. (1982) and Madariaga and Papadimitriou (1985) for simple caustics due to vertical heterogeneity. Whenever the paraxial approximation implicit in the construction of individual Gaussian beams is valid, the results of this method are very good.

THE CORNER MODEL

A more difficult model for ray theory and Gaussian beam summation is a schematic salt-dome model with sharp corners, which we call the corner model (Figure 5). The adopted frequency range (see Table 1) gives six finite-difference grids per characteristic wavelength (250 m) of the source. Some numerical grid dispersion will be apparent in the finite-difference seismograms, since the rule of thumb of 10 nodes per wavelength is not satisfied in this calculation. On the other hand, this wavelength is only one-quarter of the length of the roof of the salt dome, which is a lower limit for the validity of the high-frequency method. The main difficulties for the Gaussian beam-summation method are the sharp corners of the interface which generate diffracted waves, and the presence of creeping head waves that propagate along the interface in the higher velocity medium and continuously radiate upward into the upper layer. In the following discussion, the finite-difference results will be considered "exact."

A free interface will be sufficient for studying corner diffractions. Figure 6 presents the profiles obtained with the finite-difference (a) and Gaussian beam-summation (b) methods. The kinematic interpretation of the different arrivals in these profiles is shown at the top of Figure 5. Reflections (1) on the top of the salt dome, (2) on the lateral wall, and (3) on the horizontal interface are correctly modeled by Gaussian beam summation. Diffractions (a) and (c) by the two corners without shadow zones are approximately modeled, while diffraction (b) does not have a correct amplitude. In the backward direction, an unphysical extension of the diffracted branch (a) might be seen in front of the true diffraction. Diffraction (d) seems to be emitted by point D′ instead of point D, as shown by the shift in the arrival time. Diffractions (a′), (a″), (b′), and (c′) are not modeled by Gaussian beam summation because they are due to secondary diffraction of the already diffracted fronts (a) and (b).

A more realistic model is obtained with an interface between two elastic media. Finite-differences (a), Gaussian beam-summation (b), Maslov (c), and ray theory (d) profiles for such an example are given in Figure 7. First, we notice that the ray-theory results are correct where they can be computed, i.e., for mirror reflections (1), (2), and (3). Second, amplitudes from finite differences and Gaussian beam summation are comparable except in the zone noted in gray on the interpretation of arrival times at the top of the Figure 5. Before describing this discrepancy, we present results for reflections and diffractions.

Subcritical and postcritical reflections and diffractions can be better observed on individual seismograms for different observation positions, as shown in Figure 8. In the first seismogram, calculated at $x = .2$ km, the reflection (2) and the diffraction (c) are in perfect agreement, while the weak arrival (b) is not present in the Gaussian beam-summation seismo-

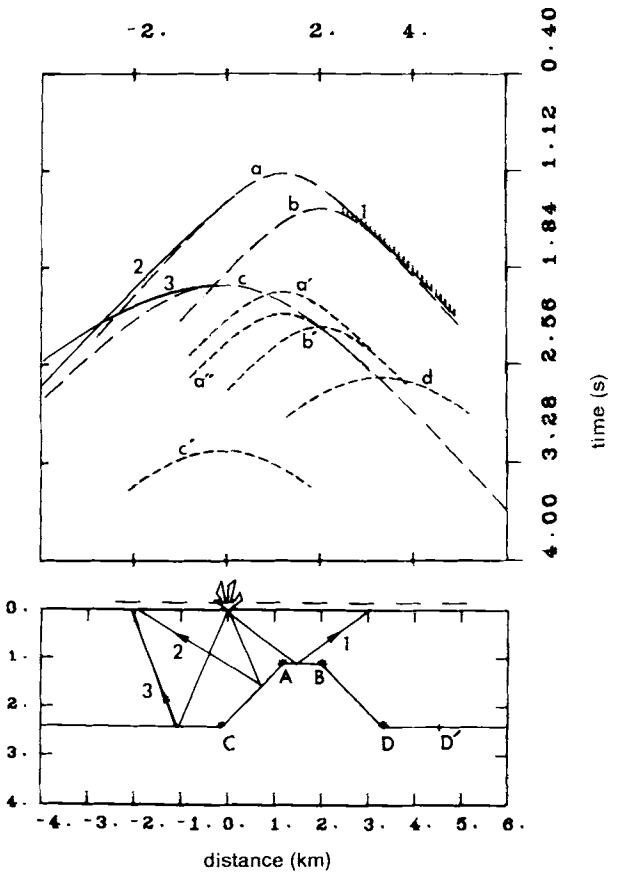

FIG. 5. Corner model: description of the different waves observed in the finite-difference profiles: specular reflections (1, 2, 3), diffractions (a, b, c) by the corners (A, B, C), and multiple diffractions (a′, a″, b′, c′, d). On the top is shown a complete set of traveltime curves, including all geometrical and diffracted arrivals.

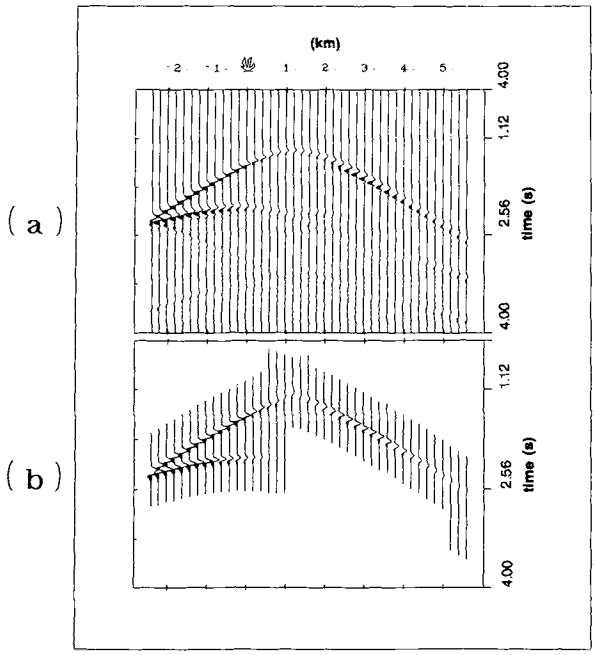

FIG. 6. Seismic profiles for the corner model, free boundary conditions at the interface. The profiles are calculated (a) by finite differences, and (b) by Gaussian beam summation.

grams. In the next seismogram, at 1.5 km, the diffraction (a) is modeled with a cutoff phase in front of it which is stronger than the true phase. The diffraction (b) is very weak for both methods. The phase (a′) cannot be modeled by the Gaussian beam-summation method because this is the secondary diffraction of an already diffracted wave. The last seismogram, at 5.2 km, shows the diffraction (d) with its arrival-time shift and a strong amplitude phase in front of it. This strong phase appears only in the finite-difference simulations. It corresponds to a creeping head wave generated at the top of the salt dome, where reflection is supercritical. When they reach the corner B of the salt dome, these creeping waves are radiated into the upper medium and contribute to the observed amplitude of the gray zone (Figure 5). These waves are not modeled by the Gaussian beam-summation method because their trajectories do not correspond to classical raypaths. Therefore they cannot be written in the simple form of equation (1).

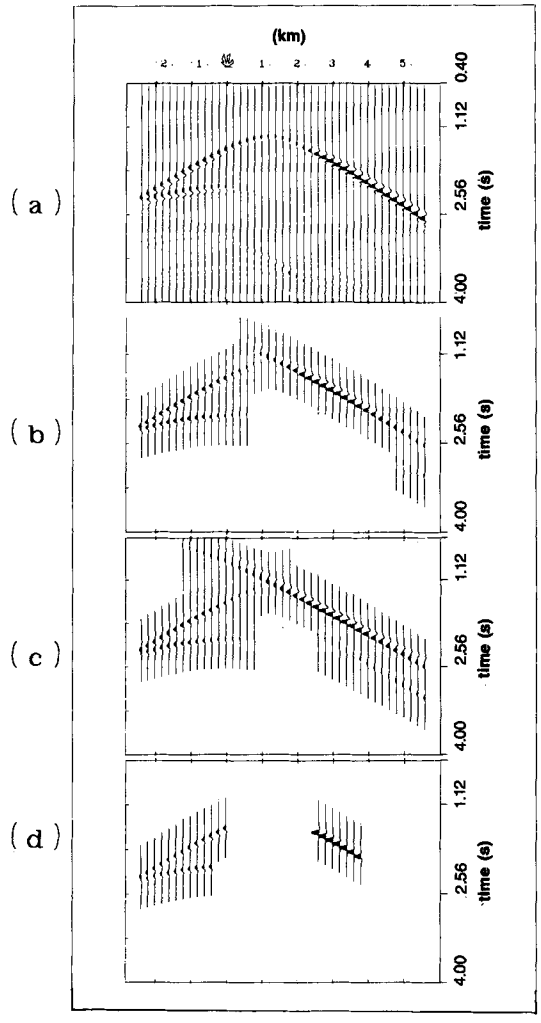

FIG. 7. Seismic profiles for the corner model, elastic half-space. The profiles are calculated (a) by finite differences, (b) by Gaussian beam summation, (c) by Maslov theory, and (d) by geometrical ray theory.

DISCUSSION AND CONCLUSION

We used finite differences and Gaussian beam summation to model reflections from complex interfaces. These two methods have very different domains of validity. The finite-difference method provides a complete solution of the wave equation, including all direct waves, reflections, and diffractions, but it is essentially a low-frequency method because the cost of solutions becomes prohibitive at high frequencies. The other method is asymptotically valid only at high frequencies because it is based on an extension of ray theory. Thus, it is particularly appropriate for modeling reflections and refractions. Its validity for computing head waves and diffractions was addressed. Comparing solutions obtained by the two methods, we attempted to determine the validity of Gaussian beam-summation solutions. In these comparisons we assumed that the finite-difference solutions were exact, although at times the rule of thumb of 10 grids per wavelength was violated. Such a comparison is not entirely accurate when evaluating the performances of the Gaussian beam-summation method since the ratio of the wavelength to the radius of curvature of the interface was only on the order of 3, which is very low for ray-theoretical methods. Nevertheless, the comparisons were very satisfactory, especially for the case of the continuous interface.

Several problems that appear in the computer implementation of the Gaussian beam method had to be solved before we could calculate the profiles presented here. The most important of these problems is the use of local coordinates determined by the geometry of the receivers. In these coordinates, it is not necessary to determine the ray-centered coordinates of every observation point with respect to every central ray to be used in the Gaussian beam summation. Except for

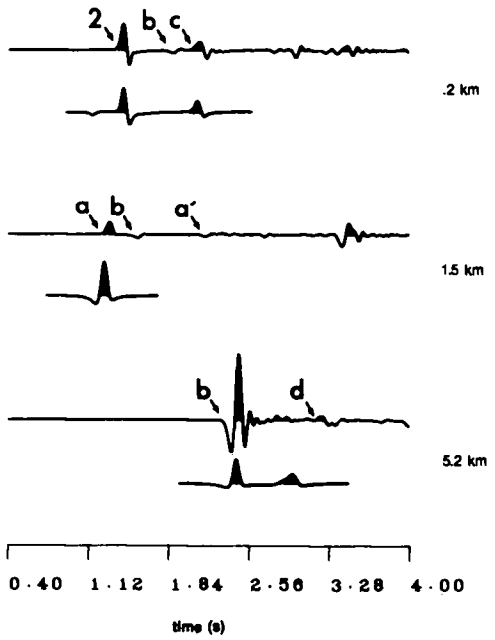

FIG. 8. Individual seismograms for the corner model with an elastic half-space calculated at three different points on the free surface. For each distance, we compare the finite-difference result (top) with the Gaussian beam-summation seismogram (below).

ray tracing, this is the most expensive and time-consuming part of the original method proposed by Červený et al. (1982). Local coordinates are also a natural way to solve the problem of calculating Gaussian beams in the vicinity of a free surface. In fact, if one wanted to use ray-centered coordinates near a boundary, a recipe for the continuation of the structure beyond the free surface would have to be provided. Another crucial point is the choice of the set of central rays used to generate individual Gaussian beams. For complex structures, the usual method of tracing rays at equal intervals of takeoff angle gives very poor results because the end points of these rays on the surface will be poorly distributed. In order to ensure a uniform approximation of the solution and to avoid problems of undersampling of the signals, it is necessary to obtain a uniform distribution of rays on the recording surface. A uniform distribution is most easily obtained using the paraxial approximation to estimate the locations of central rays in the vicinity of every recording site. The same approximation may be used to determine the most adequate spacing of rays on the recording surface for a given sampling interval in the time domain.

Two other important problems are as follows. (1) The use of an appropriate wavelet for the calculation of the beam summation is extremely important because the contribution to the beam summation is singular for beams that are very close to the recording site. A sampling function is necessary to avoid these singularities. Červený et al. (1982) proposed to use Gabor wavelets which were nearly monochromatic. We prefer to use a simple wavelet introduced by Madariaga and Papadimitriou (1985) which produces a broadening of the signal over a few time intervals which may be convolved with any desired wavelet after the summation has been evaluated. (2) The practical problem of choosing the beam-width parameter has been solved by choosing an average over a certain region on the recording surface. This avoids the usual problem of rapid variation from zero to infinity near caustics of the optimum beam width proposed by Červený et al. (1982).

The results show that Gaussian beam summation yields excellent results when the signal is strong, but it deteriorates when the observation point is in a shadow zone. In fact, Gaussian beam summation provides a reasonable approximation for diffraction at small distances from the boundary of the real wavefront, but the approximation deteriorates away from the real wavefront. This occurs mainly because the parabolic wavefronts of Gaussian beams are poor approximations to the circular wavefronts of diffracted waves. The problem is exaggerated in our profiles because of the very long wavelength that was used in order to keep finite-difference costs at a reasonable level. Another problem with Gaussian beam summation appears with conical wavefronts or head waves. In finite-difference simulations, it appears that head waves creep along the interface, following its curvature and turning around the corners. This problem is also exaggerated here because of the low frequency of the signals, but it is certainly a limitation for Gaussian beam summation. For all reflected waves, both precritical and postcritical waves, Gaussian beam summation yields excellent results, agreeing with classical ray theory when the receivers are not in the vicinity of critical points. It also gives excellent results for reverse branches and in the vicinity of caustics, where diffraction is also appropriately modeled. Thus, at a minimum extra cost when compared to geometrical ray theory, we get solutions that have a much broader range of validity. Gaussian beam summation has the additional advantages over ray theory that it does not require the use of two-point ray tracing, and that all the branches of geometrical rays arriving at a certain recorder are automatically calculated.

To compare computer costs, finite-difference simulations on 200×200 grids were done on a CRAY I computer, while all Gaussian beam summations were carried out on a PRIME 9950 minicomputer. The ratio of computer time is about 100:1. In fact, it is possible to run two-dimensional Gaussian beam calculations interactively. This is very convenient for choosing the best parameters and selecting the most appropriate set of central rays for a problem. Finally, Gaussian beam summation provides a clear interpretation of the seismic profiles in terms of wavefronts and ray trajectories. Finite-difference solutions, on the other hand, require extensive interpretation employing geometrical ray theory in order to explain the different phases that appear in the synthetic seismograms. The two methods are in fact complementary, finite differences being specially adequate at low frequencies, while Gaussian beam summation provides a very complete synthetic at high frequencies.

In conclusion, we have shown that, within its limits of validity, Gaussian beam summation gives results that compare very favorably with those obtained by finite differences, at a fraction of the cost of the latter method. The results are particularly good for strong geometrical reflections and caustics. They are poorer for diffracted arrivals and creeping head waves.

ACKNOWLEDGMENTS

This work was supported by ATP "Géophysique appliquée a la prospection" and by ATP "Centre de Calcul Vectoriel pour la Recherche no. 2250." We wish to thank Prof. V. Červený for a very enlightening discussion at a meeting in Erice, Italy, on November 1984. IPG contribution no. 945.

REFERENCES

Alford, R. M., Kelly, K. R., and Boore, D. M., 1974, Accuracy of finite-difference modeling of the acoustic wave equation: Geophysics, **39**, 834–842.

Beydoun, W., and Ben-Menahem, A., 1985, Range of validity of seismic ray and beam methods in general inhomogeneous media. II. A canonical problem: Geophys. J. Roy. Astr. Soc., **82**, 235–262.

Babich, V. M., Molotov, I. A., and Popov, M. M., 1984, Gaussian beams solutions concentrated around a line and their use: Preprint, Inst. Radiotech. and Electron. (in Russian).

Babich, V. M., and Pankratova, T. F., 1973, On discontinuities of the Green function of mixed problems for wave equations with variable coefficients: Prob. Math. Phys., **6**, 9–27.

Červený, V., 1983, Synthetic body-wave seismograms for laterally varying layered structures by the Gaussian beam method: Geophys. J. Roy. Astr. Soc., **73**, 389–426.

Červený, V., and Hron, F., 1980, The ray-series method and dynamic ray tracing for three-dimensional in inhomogeneous media: Bull., Seis. Soc. Am., **70**, 47–77.

Červený, V., and Klimes, L., 1984, Synthetic body wave seismograms for three dimensional laterally varying media: Geophys. J. Roy. Astr. Soc., **79**, 119–133.

Červený, V., Popov, M. M., and Pšenćik, I., 1982, Computation of wave fields in inhomogeneous media—Gaussian beam approach: Geophys. J. Roy. Astr. Soc., **70**, 109–128.

Červený, V., and Pšenćik, I., 1984, Gaussian beams in elastic 2-D

laterally varying layered structures: Geophys. J. Roy. Astr. Soc., **78**, 65–91.
Chapman, C. H., and Drummond, R., 1982, Body-wave seismograms in inhomogeneous media using Maslov asymptotic theory: Bull., Seis. Soc. Am., **52**, S277–S317.
Cisternas, A., Jobert, G., and Compte, P., 1984, Classical theory of Gaussian beams (in Spanish): Rev. de Geofis., **40**, 27–32.
Katchalov, A. P., and Popov, M. M., 1981, The application of the Gaussian beams summation method to the computation of wave fields in the high-frequency approximation: Dokl. Akad. Nauk.
Madariaga, R., 1984, Gaussian beam synthetic seismograms in a vertically varying medium: Geophys. J. Roy. Astr. Soc., **79**, 589–612.
Madariaga, R., and Papadimitriou, P., 1985, Gaussian beam modelling of upper mantle phases: Annal. Geophys., **3**, 799–812.
Nowack, R., and Aki, K., 1984, The 2-D Gaussian beam synthetic method: testing and application: J. Geophys. Res., **89**, 7797–7819.
Virieux, J., 1984, *SH*-wave propagation in heterogeneous media: Velocity-stress finite-difference method: Geophysics, **49**, 1933–1957.
——— 1986, *P-SV* wave propagation in heterogeneous media: Velocity-stress finite-difference method: Geophysics, **51**, 889–901.